EVIDENCE FOR LINE BROADENING BY ELECTRON SCATTERING IN THE BROAD LINE REGION OF NGC 4395

Ari Laor

Physics Department, Technion, Haifa 32000, Israel
Draft version February 5, 2008

ABSTRACT

A high quality Keck spectrum of the Hα line in NGC 4395 reveals symmetric exponential wings, $f_v \propto e^{-v/\sigma}$, with $\sigma \simeq 500$ km s^{-1}. The wings extend out to $\gtrsim 2500$ km s^{-1} from the line core, and down to a flux density of $\lesssim 10^{-3}$ of the peak flux density. Numerical and analytic calculations indicate that exponential wings are expected for optically thin, isotropic, thermal electron scattering. Such scattering produces exponential wings with $\sigma \simeq 1.1\sigma_e(\ln \tau_e^{-1})^{0.45}$, where σ_e is the electron velocity dispersion, and τ_e is the electron scattering optical depth. The Hα wings in NGC 4395 are well fit by an electron scattering model with $\tau_e = 0.34$, and an electron temperature $T_e = 1.1 \times 10^4$K. Such conditions are produced in photoionized gas with an ionization parameter $U \simeq 0.3$, as expected in the broad line region (BLR). Similar analysis of the [O III] λ5007 line yields $\tau_e < 0.01$, consistent with the lower ionization in the narrow line region. If the electron scattering interpretation is correct, there should be a tight correlation between τ_e and the ionizing flux on time scales shorter than the BLR dynamical time, or ~ 1 week for NGC 4395. In contrast, the value of σ should remain nearly constant on these time scales. Such wings may be discernible in other objects with unusually narrow Balmer lines, and they can provide a useful direct probe of T_e and τ_e in the BLR.

Subject headings: galaxies: active — galaxies: Seyfert — quasars: emission lines — galaxies: individual
NGC 4395

1. INTRODUCTION

Early studies of the broad line profiles in Type 1 Active Galactic Nuclei (AGN) suggested that the large observed line widths ($\gtrsim 3000$ km s^{-1}) are produced by electron scattering within the photoionized gas (Weymann 1970; Mathis 1970). With the development of photoionization models for the Broad Line Region (BLR), it was however realized that the expected electron scattering optical depth, τ_e, within the BLR gas is $\ll 1$, which is too low to explain the observed line profiles (Davidson & Netzer 1979). Later studies of the size of the BLR, based on reverberation mappings, indicated that the BLR is more compact than previously thought (e.g. Rees, Netzer, & Ferland 1989), and thus τ_e is expected to be higher than previously thought, though it is not expected to reach $\tau_e > 1$, required to explain the line profiles purely by electron scattering. There is also good evidence now that the line broadening in the BLR is mostly due to virialized bulk motion (e.g. Peterson & Wandel 2000). However, electron scattering by a significantly hotter gas outside the BLR gas ($T \sim 10^{6-7}K$ vs. $T \sim 10^4 K$) remains a viable option (Shields & McKee 1981; Kallman & Krolik 1986; Emmering et al. 1992; Bottorff et al. 1997). Evidence for electron scattering of continuum photons in AGN is provided by wavelength independent polarization in some objects (e.g. Antonucci et al. 1993), but there is yet no conclusive detection of electron scattering effects on the broad line profiles.

A possible exception may occur in NGC 1068, where spatially resolved spectropolarimetry reveals a broadened Hα line, which may result from electron scattering in warm ($T \sim 10^5 K$) gas (Miller, Goodrich & Mathews 1991). A spectropolarimetric search for polarized broad lines in low luminosity AGN (Barth et al. 1999) revealed a polarized BLR component in the lowest luminosity type I AGN, NGC 4395. Based on that detection, Barth et al. suggested that higher S/N spectropolarimetry may reveal a broadened Hα component, if the polarization is induced by electron scattering. Here we report on a high quality Keck observation of the Hα line in NGC 4395, which indeed reveals extended symmetric exponential wings (though their polarization is unknown). As shown below, these wings are well fit by optically thin electron scattering by electrons at $T_e = 1.14 \times 10^4 K$, with $\tau_e = 0.34$, which are plausible conditions for the BLR gas.

The paper is structured as follows. Section 2 describes the observations which revealed the exponential wings in the Hα profile of NGC 4395. Section 3 describes the numerical calculation of the electron scattering line profiles, which yield exponential wings, $f_v = f_0 e^{-v/\sigma}$. A fitting formula for σ as a function of T_e and τ_e is provided, together with a simple analytic derivation. In section 4 the observed Hα profile is fit with the electron scattering model, yielding T_e and τ_e, the origin of the scattering gas is discussed, and some predictions are made. The main conclusions are summarized in section 5.

2. OBSERVATIONS

NGC 4395 was observed with the Keck-II 10 m telescope using the Echellette Spectrograph and Imager (ESI; Sheinis et al. 2002); a slit width of 0".5, and a spectral resolution of $\lambda/\Delta\lambda = 8,000$, or 0.820 Å near Hα, sampled at 0.259 Å per pixel. Two 20 minute exposures were made on 2002 December 2 UT, yielding a S/N ranging from 50 per pixel at the continuum near Hα to 400 at the line peak (for the reduction details see Laor et al. 2006).

Electronic address: laor@physics.technion.ac.il

arXiv:astro-ph/0601688v1   30 Jan 2006

The continuum level is estimated using a linear fit to the observed flux densities of 4.32×10^{-16} erg s^{-1} cm^{-2} Å^{-1} at observed frame 6480 Å, and 4.20×10^{-16} erg s^{-1} cm^{-2} Å^{-1} at 6640 Å. The implied spectral slope of $f_\lambda \propto \lambda^{-1.15}$ between 6480 Å and 6640 Å is consistent with the global optical continuum spectral slope in the ESI spectrum, although the flux at 6640 Å appears to be somewhat blended with the extended blue wing of the He I $\lambda6678.15$ line. We estimate the continuum placement uncertainty as $\sim 3 \times 10^{-18}$ erg s^{-1} cm^{-2} Å^{-1}. This uncertainty implies a potential systematic error of $\sim 10\%$ in the net line flux at $|v| = 2500$ km s^{-1}, increasing to $\sim 100\%$ at $|v| = 3000$ km s^{-1}. We therefore consider the Hα line profile reliable at $|v| < 2500$ km s^{-1}, where any systematic flux error is $< 10\%$. The continuum 1 σ noise level per pixel is 9.5×10^{-18} erg s^{-1} cm^{-2}, and thus the statistical uncertainty per pixel is $\sim 30\%$ at $|v| = 2500$ km s^{-1}. We find a S/N> 10 per resolution element at $|v| < 2000$ km s^{-1}, increasing to > 70 at $|v| < 1000$ km s^{-1}. Overall, the high quality of the ESI spectrum allows us to reliably probe the Hα profile over an unprecedented range of a factor of 1000 in flux density, from 3.58×10^{-14} erg s^{-1} cm^{-2} Å^{-1} at $v = 0$ km s^{-1} to $\sim 3 \times 10^{-17}$ erg s^{-1} cm^{-2} Å^{-1} at $|v| = 2500$ km s^{-1}.

Figure 1, upper panel, presents the overall Hα line profile at $|v| < 3000$ km s^{-1}. The nearly pure linear shape in log f_E versus v is very prominent, implying exponential wings. The middle panel demonstrates the asymmetry present in the $|v| < 1000$ km s^{-1} region of the broad line profile, with excess blue wing flux. Note that the wings at $|v| > 1000$ km s^{-1} show an opposite asymmetry (see upper panel), however there is a very good match of the red and blue wings when the spectrum is reflected with respect to the $v = 50$ km s^{-1} point (lower panel). The two wings are well matched by an exponential profile, $f_E \propto e^{-v/\sigma}$, with $\sigma = 500$ km s^{-1}. These pure symmetric exponential wings suggest a scattering origin. Below we show that exponential wings are indeed a generic prediction of optically thin isotropic electron scattering.

3. CALCULATIONS

3.1. *Numerical*

A complete calculation of electron scattering line profiles involves a calculation of the photon diffusion simultaneously in both real space and in energy space. Such a calculation can be carried out using a Monte Carlo approach, which is straightforward to implement, though the finite number of photons used tends to produce non smooth curves (e.g. Lee 1999) compared to analytic solutions. Analytic solutions for the local diffusion in space, described by the radiative transfer equation, and diffusion in energy, described by the energy redistribution function, have been derived and solved numerically using various simplifying assumptions (e.g. Chandrasekhar 1960; Mihalas 1978; and references therein). Here we make two major simplifying assumptions. First, the electron scattering gas is assumed to be optically thin, thus a detailed radiative transfer solution is not required. This simplification is justified by the observation that the dominant effect on the line broadening in the BLR appears to be gravity dominated bulk motion, rather than electron scattering. Gravity is indicated by the good cor-
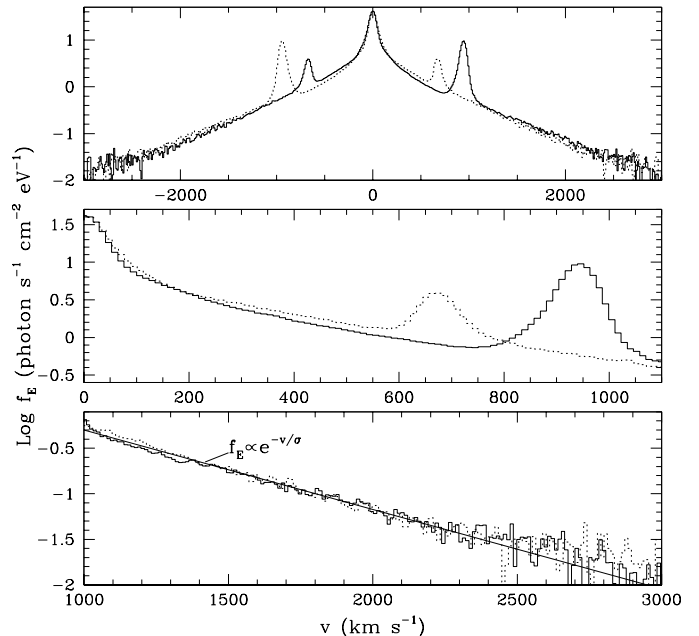

FIG. 1.— Upper panel: The observed Hα profile in NGC 4395 (solid histogram), and the reflected profile (dotted histogram). Note that the blue wing is higher than the red wing at $|v| < 1000$ km s^{-1}, while the reverse is true at $|v| > 1000$ km s^{-1}. Middle panel: An expanded view of the line core. The narrow Hα line dominates at $|v| < 150$ km s^{-1}, and the narrow [N II] lines dominate around $v \sim 950$ km s^{-1}, and $v \sim -670$ km s^{-1}. Lower panel: An expanded view of the extended wings at $1000 < |v| < 3000$ km s^{-1}. The velocity scale in this panel was shifted from v to $v-50$ km s^{-1}. Note the remarkable symmetry of the wings in the shifted scale, and their nearly pure exponential form. The solid line is an exponential function with $\sigma = 500$ km s^{-1}.

respondence between black hole mass estimates assuming a virialized BLR and mass estimates based on the host bulge properties (Laor 1998; Ferrarese et al. 2001). Second, we assume an isotropic electron velocity distribution, and an isotropic illumination of the scattering electrons, which is likely to be a good approximation for the integrated scattered radiation. These assumptions lead to the following remarkably simple energy redistribution function, derived by Rybicki & Lightman (1979, hereafter RL79. Eq. 7.24 there),

$$j(x,\beta) = \frac{1-\beta^2}{4\beta^2}[(1+\beta)x - (1-\beta)] \quad \text{for} \quad \frac{1-\beta}{1+\beta} < x < 1 \tag{1}$$

$$j(x,\beta) = \frac{1-\beta^2}{4\beta^2}[(1+\beta) - x(1-\beta)] \quad \text{for} \quad 1 < x < \frac{1+\beta}{1-\beta}, \tag{2}$$

$$j(x,\beta) = 0 \quad \text{for} \quad x > \frac{1+\beta}{1-\beta} \quad \text{or} \quad x < \frac{1-\beta}{1+\beta}, \tag{3}$$

where $x \equiv e/e_0$, and e_0, e are the observed photon energy before and after scattering, $v = \beta c$ is the scattering electron velocity, and $j(x,\beta)$ is the number of photons scattered per dx, which obeys the photon conservation $\int_0^\infty j(x,\beta)dx = 1$. The expressions above for $j(x,\beta)$ apply for elastic scattering in the electron rest frame, which
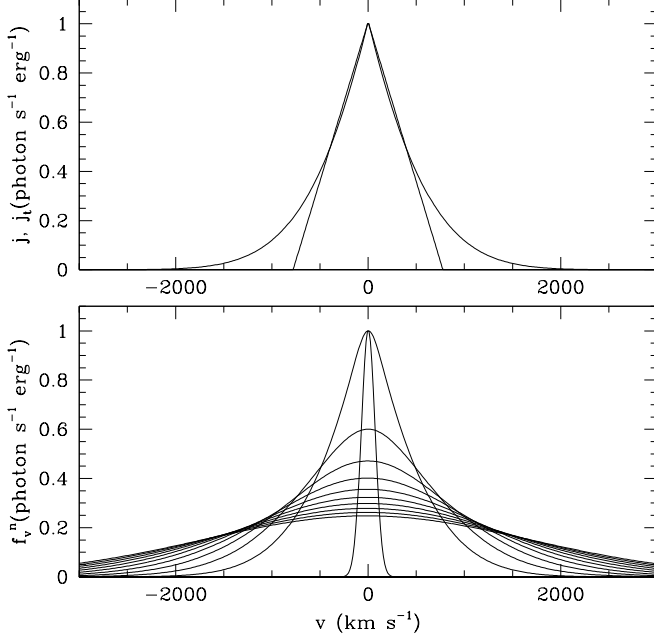
FIG. 2.— Upper panel: The single velocity redistribution function $j(x, \beta)$ for $T_e = 10^4$ K (triangle shaped curve), and the thermal averaged function $j_t(x)$, scaled to match $j(x, \beta)$ at $x = 1$ (i.e. at $v = 0$ km s^{-1}). Note that despite the thermal averaging the core of the redistribution function is almost unchanged. Lower panel: The effects of repeated scattering. The narrow Gaussian is the unscattered line profile, and the broader curves correspond to f_v^n with $n = 1 - 10$. The number of photons (area under each curve) is assumed to be conserved, and the unscattered line profile was scaled to match the peak of the $n = 1$ curve.

FIG. 3.— The dependence of $f_v^{\rm scat}$ on T_e and τ_e. Upper panel: The dependence on T_e for $\tau_e = 0.3$. The line wings approach a linear shape in log $f_v^{\rm scat}$ versus v, i.e. an exponential form $f_v^{\rm scat} \propto e^{-v/\sigma}$, at high v. Note that σ increases significantly with T_e. Lower panel: The dependence on τ_e for $T_e = 2 \times 10^4$ K. The integrated scattered flux is proportional to τ_e, however σ is only weakly dependent on τ_e.

is a very good approximation for the applications below, where $\beta \ll 1$ and $h\nu \ll m_e c^2$.

To obtain the redistribution function for a thermal electron distribution, $j_t(x)$, one needs to integrate the above expression for $j(x, \beta)$ over a thermal velocity distribution function. Thus

$$j_t(x) = \frac{4}{b^3 \sqrt{\pi}} \int_0^\infty j(x, \beta) v^2 e^{-(v/b)^2} dv \qquad (4)$$

where $b \equiv 2kT_e/m_e$, and T_e is the electron temperature. Figure 2 (upper panel) shows $j(x, \beta)$ and $j_t(x)$. Note that despite the thermal averaging, $j_t(x)$ remains sharply peaked.

Since the scattering medium is optically thin, each scattering redistributes the observed line profile through $j_t(x)$, and reduces the number of photons by a factor of τ_e. Thus, the line profile following $n + 1$ scattering is given by a convolution of $j_t(x)$ with the n times scattered profile, i.e.

$$f_v^{(n+1)} = \tau_e \int_0^\infty f_{v'}^n j_t[(v - v')/c] dv' \qquad (5)$$

where f_v^n is the profile of a line scattered n times. Since $\beta \ll 1$, a simple Doppler relation $de/e_0 = dv/c$ can be assumed. Figure 2 (lower panel) shows f_v^0, an arbitrary seed line profile, and f_v^n for $n = 1 - 10$, illustrating how the line gets broader and shallower with repeated scattering by a given electron population. The total scattered
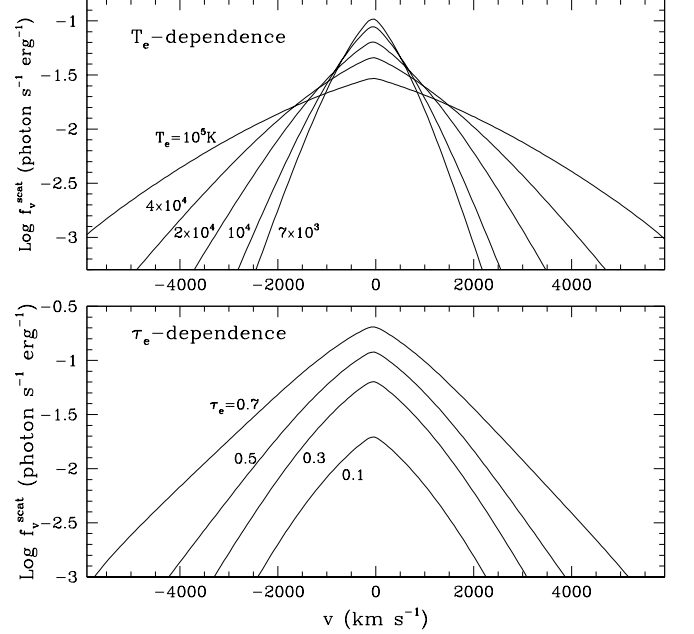
line profile is then given by

$$f_v^{\rm scat} = \sum_{n=1}^\infty f_v^n. \qquad (6)$$

Figure 3 shows the results of numerical calculations of $f_v^{\rm scat}$ for a range of T_e and τ_e values. As both T_e and τ_e increase, the line profile gets broader, with a relatively weak dependence of the width on τ_e and a stronger dependence on T_e. Note that in all cases log $f_v^{\rm scat}$ approaches a linear function of v in the extended wings, or equivalently

$$f_v^{\rm scat} = f_0 e^{-v/\sigma}. \qquad (7)$$

Figure 4 shows a plot of σ, measured from the numerical calculations, as a function of τ_e and T_e. The solid lines is a fit to the numerical results. The fitting function has the simple form,

$$\sigma = 1.1\sigma_e (\ln \tau_e^{-1})^{-0.45}, \qquad (8)$$

where σ_e is the thermal electron velocity dispersion,

$$\sigma_e = \sqrt{kT_e/m_e} = 389.2 T_4^{1/2} \text{ km s}^{-1}, \qquad (9)$$

and $T_4 \equiv T_e/10^4$. This fitting function is accurate to 1.5% in the range $0.01 \le \tau_e \le 0.8$.

3.2. Analytic Derivations

3.2.1. An Oversimplified Derivation

One may attempt to understand the above fit equation based on the following very simple derivation. This derivation is actually oversimplified, and the resulting

expression for σ lacks accuracy, but it provides insight for understanding the basic reason for the formation of exponential profile wings.

This derivation follows closely the derivation of the power law spectral form produced through optically thin electron scattering by relativistic electrons, as described in RL79 (section 7.5 there). Here we have optically thin electron scattering by non relativistic electrons. Let σ_e be the mean electron velocity. The energy amplification of a photon scattered at right angle is

$$e_1/e_0 \simeq 1 + \sigma_e/c. \tag{10}$$

After n such scattering the photon energy will be

$$e_n \simeq e_0(1 + \sigma_e/c)^n, \quad \text{or} \quad e_n \simeq e_0(1 + n\sigma_e/c), \tag{11}$$

where the last step is valid for $n\sigma_e/c \ll 1$. Changing to velocity scale

$$v_n \equiv (e_n/e_0 - 1)c, \quad \text{gives} \quad v_n \simeq n\sigma_e. \tag{12}$$

The fraction of photons scattered n times is τ_e^n, and thus

$$f(v_n) \simeq f(0)\tau_e^n, \quad \text{or} \quad f(v_n) \simeq f(0)\tau_e^{v_n/\sigma_e}. \tag{13}$$

This is equivalent to

$$f(v_n) \simeq f(0)e^{\ln \tau_e v_n/\sigma_e}, \tag{14}$$

i.e. an exponential line profile, where

$$f(v) \propto f(0)e^{-v/\sigma} \quad \text{and} \quad \sigma = \sigma_e/\ln \tau_e^{-1}. \tag{15}$$

The crucial difference here from relativistic electron scattering is that the energy increment with repeated scattering is a constant linear factor, rather than a constant multiplicative factor, which would lead to a power law rather than an exponential form.

The above derivation of σ does not yield the correct dependence on $\ln \tau_e$. The oversimplification in the above derivation is in the assumption that the energy redistribution function can be approximated as a δ function at $e_1/e_0 \simeq 1 + \sigma_e/c$, while as Eqs.1-3 above show, the photons actually get redistributed nearly symmetrically from $1 - \sigma_e/c$ to $1 + \sigma_e/c$. For highly relativistic electrons the strong Doppler beaming produces a highly asymmetric and strongly peaked redistribution function (at $e_1/e_0 \simeq \gamma^2$), and the simplified derivation of the power law spectral slope through repeated scattering (RL79) is adequate.

3.2.2. A Simplified Derivation

Taking into account the shape of the redistribution function leads to a more accurate dependence of σ on τ_e, as described below.

The thermal redistribution function can be approximated as a Gaussian with the velocity dispersion of the scattering electrons, $j_t(x) \propto e^{-v^2/b^2}$. The seed line profile is assumed to have a smaller velocity width than that of the scattering electrons, so it can be conveniently approximated as a δ function, $f_v^0 = \delta(v)$. Thus, the first scattering (Eq.5) yields $f_v^1 = j_t(x)$, and repeated scattering amount to repeated convolutions with $j_t(x)$. Such convolutions yield Gaussians with a velocity dispersion which grows as $\sqrt{n}$, i.e. we can use the approximation

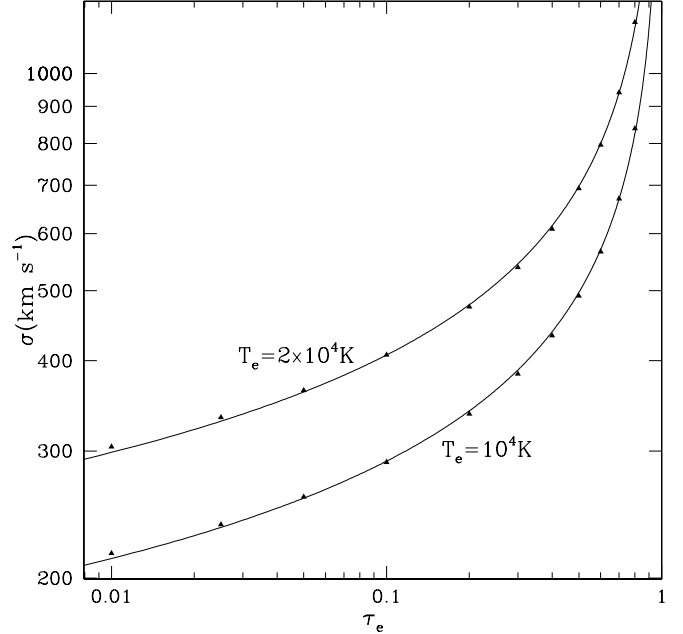$$f_v^n = K\frac{\tau_e^n}{\sqrt{n}}e^{-v^2/nb^2}, \tag{16}$$

FIG. 4.— The dependence of σ on τ_e for two values of T_e. The filled triangles are values measured from numerical calculations of f_v^{scat}, and the solid lines are analytic fits of the form $\sigma = 1.1\sigma_e(\ln \tau_e^{-1})^{-0.45}$ to the numerical results (see text). This fit is accurate to 1.5% in the displayed range.

where K is an arbitrary constant, and the $1/\sqrt{n}$ term comes from the Gaussian normalization. The total scattered line profile is then given by

$$f_v^{\text{scat}} = K\sum_{n=1}^{\infty} \frac{\tau_e^n}{\sqrt{n}}e^{-v^2/nb^2}. \tag{17}$$

Unfortunately, there is no simple analytic solution for the sum of this series. Note, however, that only a few terms in the above series contribute at any given v. The contribution of terms with $n \ll v^2/b^2$ is small because of the large negative exponential factor, while the contribution of terms with $n \gg v^2/b^2$ is reduced by the $\tau_e^n/\sqrt{n}$ factor. The maximum contribution to f_v^{scat} in the above sum is provided by the term $n_{\max}$, which is obtained from the requirement

$$\frac{df_v^n}{dn} = (\ln \tau_e - \frac{1}{2n} + \frac{v^2}{n^2b^2})f_v^n = 0, \tag{18}$$

which holds at $n = n_{\max}$. Since $f_v^n \neq 0$ one gets a quadratic equation for $n_{\max}$

$$n_{\max}^2 - \frac{n_{\max}}{2\ln \tau_e} + \frac{v^2}{b^2\ln \tau_e} = 0. \tag{19}$$

The second term can be neglected compared to the first and third terms when $n > 1$ and $\tau_e < 0.6$. Thus, the solution is

$$n_{\max} = \frac{v}{b\sqrt{\ln \tau_e^{-1}}}. \tag{20}$$

Substituting $n_{\max}$ in the general expression for f_v^n gives

$$f_v^{n_{\max}} = K\frac{e^{-2v\sqrt{\ln \tau_e^{-1}}/b}}{\sqrt{v/(b\sqrt{\ln \tau_e^{-1}})}}. \tag{21}$$

We further show that f_v^n indeed has a narrow peak around $n = n_{\max}$. We define the peak width, Δn, through the relation $f_v^{n_{\max}+\Delta n}/f_v^{n_{\max}} = 0.5$, which yields after some steps the condition

$$\tau_e^{2(\Delta n)^2/n} \simeq 0.5, \qquad (22)$$

or

$$\Delta n \simeq 0.6 n^{1/2}/\sqrt{\ln \tau_e^{-1}}, \qquad (23)$$

i.e. only the nearest 1-2 bins to $n_{\max}$ contribute significantly for $n \lesssim 10$. Thus, at each v one can approximate the above sum over n by just a single term at $n = n_{\max}$, i.e. $f_v^{\mathrm{scat}} = f_v^{n_{\max}}$. To verify that f_v^{scat} has the correct exponential form we calculate

$$\frac{1}{\sigma} = \frac{d \ln f_v^{\mathrm{scat}}}{dv} = \frac{2\sqrt{\ln \tau_e^{-1}}}{b} - \frac{1}{2v}. \qquad (24)$$

Thus, a pure exponential line profile, i.e. σ independent of v, is obtained when the second term on the right is negligible, which occurs at $v > b/4\sqrt{\ln \tau_e^{-1}}$. The exponential slope is $\sigma = b/2\sqrt{\ln \tau_e^{-1}}$, or $\sigma = 0.71\sigma_e\sqrt{\ln \tau_e^{-1}}$, which matches well the $\ln \tau_e$ dependence of the fitting function to the numerical solution (Eq.8).

4. RESULTS AND DISCUSSION

4.1. *The best fit electron scattering model*

To model the shape of the electron scattering wings one needs an estimate of the seed line profile. As shown below, there is no evidence for detectable electron scattering wings for lines originating in the narrow line region (NLR), and we therefore use only the broad component of Hα for the seed profile. To obtain the BLR Hα component, we subtract off the narrow Hα component and the narrow [N II] lines from the observed Hα profile. The broad component underlying the narrow lines is interpolated using a spline fit, where we use the minimum number of spline points required to get both an acceptable χ^2, and also matching profiles for the narrow [N II] doublet lines (Laor et al. 2006).

The observed broad line core at $|v| < 1000$ km s^{-1} shows a noticeable asymmetry, with up to $\sim 50\%$ higher flux in the blue wing (Fig.1, middle panel). This appears to be a persistent effect in NGC 4395, as it is also present in high resolution Keck spectra taken about a year and eight years earlier (Fig.1 in Laor et al. 2006). In contrast, the wings at $|v| > 1000$ km s^{-1} are generally symmetric to $< 10\%$ (with respect to $v = 50$ km s^{-1}, Fig.1, lower panel). Since our electron scattering model generates symmetric line profiles, one must assume that the observed asymmetric core profile represents the unscattered seed line. To estimate the shape of the seed line wings, the observed profile is multiplied by a weight function of the arbitrary functional form e^{-v^2/w^2}, which produces a smooth cutoff in the the wings at $|v| > w$. We find that $w = 600$ km s^{-1} at $v > 0$ km s^{-1}, and $w = 800$ km s^{-1} at $v < 0$ km s^{-1}, are about the minimum values required to exclude the inner asymmetric core emission, and allow the electron scattering model to fit only the extended symmetric wings. The exact value of w cannot be accurately constrained, and the true seed profile may be broader than assumed here. The seed profile is further multiplied by $e^{-\tau_e}$, which represents the

wavelength independent suppression due to the electron scattering, where τ_e is determined below.

The seed line profile obtained above is now used as the input line profile for our electron scattering code. The model free parameters are T_e and τ_e, and we iterate over different values for these parameters until a satisfactory fit is obtained between the observed broad Hα profile, and the sum of the scattered + seed line profiles (see Figure 5). The scattering medium is assumed to have a bulk velocity of $v = 50$ km s^{-1}, with respect to the narrow line peak, as suggested by the observed asymmetry of the extended wings. The best fit is obtained for $T_e = 1.14 \times 10^4$ K, and $\tau_e = 0.34$, which yields $\chi^2 = 282$ for 243 degrees of freedom, where χ^2 is calculated for $|v| < 2500$ km s^{-1}, excluding the line core region, $-900 < v < 1200$ km s^{-1}, affected by the narrow lines. The best fit T_e and τ_e depend on the assumed shape for the seed line profile. Increasing the wings cutoff velocity, w, reduces the best fit τ_e and increases T_e. For example, adopting $w = 1200$ km s^{-1} yields a best fit solution with $T_e = 1.7 \times 10^4$ K, and $\tau_e = 0.17$. However, at such a high w the seed line contribution becomes negligible ($< 20\%$ of total line flux) at $|v| \gtrsim 1500$ km s^{-1}, compared to $|v| \gtrsim 1000$ km s^{-1} for the minimum w solution. The observed wings are well fit by a featureless exponential profile already at $|v| \gtrsim 1000$ km s^{-1} (Fig.1, lower panel), which suggests this region is dominated by a single component, as we find for the minimum w solution. We therefore adopt below the best fit minimum w solution, although one cannot rule out a higher w solution, where the seed line profile and the scattered wings conspire to produce a single featureless exponential profile at $|v| \gtrsim 1000$ km s^{-1}.

Once the seed line profile is set, there is essentially no degeneracy in the solution, as τ_e is fixed uniquely by the ratio of seed to scattered photon flux ratio, and T_e is then fixed by τ_e and the observed exponential slope, σ. The formal uncertainties in T_e and τ_e due to the available S/N here are $\leq 3 - 5\%$. However, our assumption of an isothermal and isotropic scattering medium may be a significant oversimplification, and systematic errors $\gtrsim 10\%$ are quite possible due to our simplified modeling.

4.2. *Where does the scattering takes place?*

The best fit T_e is typical of photoionized gas in the BLR or the NLR. To clarify whether the scattering gas resides in the BLR or in the NLR, we looked for evidence for electron scattering wings in the profile of the [O III] $\lambda5007$ line, the strongest narrow line in the spectrum of NGC 4395. Figure 6 shows the continuum subtracted line profile. Weak broad wings appear to be present at $|v| > 500$ km s^{-1}. To determine the implied τ_e, one needs an estimate of the seed line profile. As for the Hα line, we multiplied the observed profile by a weight function of the form e^{-v^2/b^2}, using here $b = 400$ km s^{-1}. We fixed T_e at 1.14×10^4 K, the value measured for Hα, and obtained a reasonable fit to the wing profile using $\tau_e = 0.01$. However, weak broad wings are also present in the instrumental line spread function (LSF) at a level of $\sim 10^{-3}$ of the peak line flux density. Convolving the seed [O III] $\lambda5007$ line profile with the instrumental LSF produces wings which are also roughly consistent with the observed wing flux (Fig.6). We thus conclude that
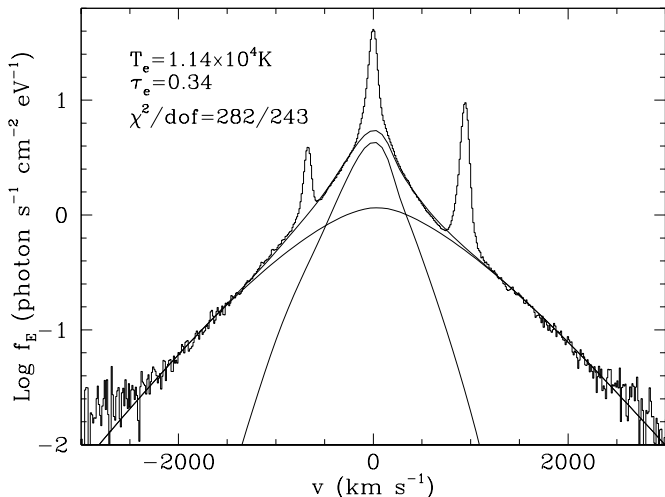
FIG. 5.— The observed Hα profile (solid histogram), and the best fit optically thin electron scattering model (solid line). The input seed line profile and the electron scattered profile are also shown. The best fit parameters and the fit χ^2 are indicated on the plot.
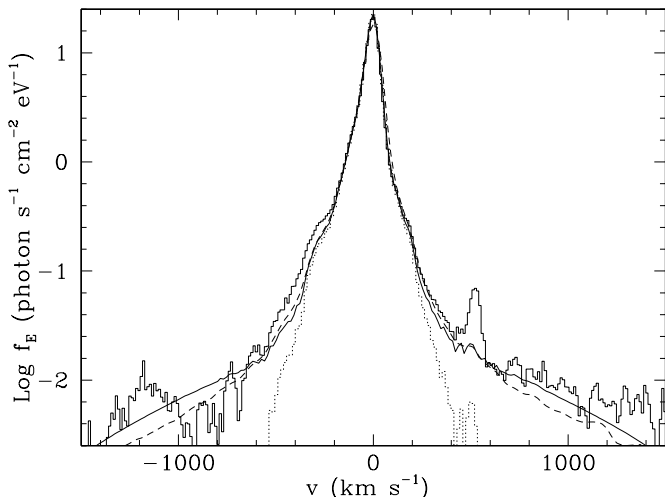

FIG. 6.— The observed [O III] λ5007 line profile (solid histogram), the assumed seed line profile (dotted histogram)), and the best fit optically thin electron scattering model (solid line) having $\tau_e = 0.01$ and T_e fixed at 1.14×10^4 K. The wings are also consistent with instrumental broadening (dashed line), and therefore we deduce that $\tau_e < 0.01$. The feature at $v \sim 500$ km s^{-1} is the He I λ5015.68 line.

most, or possibly all, of the [O III] λ5007 wing flux may be instrumental, and therefore one can only put an upper limit of $\tau_e < 0.01$ on a $T_e \simeq 10^4$ K scattering medium at, or outside, the NLR.

In contrast to the [O III] λ5007 line, the instrumental LSF has a negligible effect on the Hα line wings. For example, the instrumental LSF, acting on the narrow Hα component, produces a flux density at $|v| = 1500$ km s^{-1} which is $< 10^{-4}$ of the peak flux density (Fig.6), while the observed Hα flux density at $|v| = 1500$ km s^{-1} is $\sim 5 \times 10^{-3}$ of the peak flux density (Fig.5). In addition, the instrumental LSF scatters only $\sim 1\%$ of the line flux into broad wings, while the observed broad wings flux

in Hα amounts to 34% of the line flux, again indicating that the exponential Hα wings cannot be an instrumental effect.

Since the [O III] λ5007 line shows no scattering wings, the scattering wings of Hα must originate in gas at radii smaller than the NLR, most plausibly within the photoionized gas which produces the BLR emission lines. An optical depth $\tau_e = 0.34$ implies an electron column of 5.1×10^{23} cm^{-2}, or equivalently a minimum total H column of about 4.6×10^{23} cm^{-2}. Photoionized gas typically has an ionized, H II, surface layer with a column of $\Sigma_{\rm ion} \approx 10^{23}U$ cm^{-2}, where $U \equiv n_\gamma/n_e$ is the ionization parameter, and n_γ and n_e are (respectively) the H ionizing photon and the electron number densities. To yield the required τ_e within this surface layer requires $U \sim 5$. This value of U is much larger than the typical $U \sim 0.1$ at the BLR, and it implies $T_e \simeq 5 \times 10^4$ K within the H II layer. Such a high T_e is clearly excluded by our measurement of $T_e = 1.14 \times 10^4$ K within the Hα scattering layer. However, below the surface H II layer lies an extended layer of partially ionized gas, where the lower ionization lines (Mg II, Fe II), and most of the Balmer lines originate. The Hα scattering wings may therefore originate in this deeper layer.

The ionization structure of the partially ionized layer cannot be deduced by simple arguments, as made above for the H II layer. We therefore use the photoionization code CLOUDY (Ferland et al. 1998) to calculate τ_e, as a function of U and total column $\Sigma_{\rm H}$, for models with a significant H I column. The partially ionized layer is heated by the harder, more penetrating radiation. We assume a spectral energy distribution (SED) having an energy spectral slope of -1 from 1 eV to 10 eV, -1.5 from 10 eV to 1 keV, -0.2 from 1 keV to 40 keV, and a cutoff above 40 keV, which is consistent with the SED measured for NGC 4395 by Moran et al. (1999). This X-ray hard SED produces about twice the τ_e obtained for the softer Mathewes & Ferland (1987) SED, commonly used for photoionization calculations. The observed $\tau_e = 0.34$ is obtained for $\Sigma_{\rm H} = 10^{24}$ cm^{-2} and $U = 0.3$, well within the plausible range for the BLR. The CLOUDY model calculations show there is a significant temperature gradient within the electron scattering layer. The surface temperature is 3.4×10^4 K, dropping to 1.6×10^4 K at a depth where $\tau_e = 0.07$, 7.2×10^3 K at $\tau_e = 0.19$, and 7×10^3 K at $\tau_e = 0.3$. Calculating the electron scattering profile of a nonisothermal slab requires a complete radiation transfer calculation, including the Hα emissivity as a function of depth, which is well beyond the scope of this paper. However, our isothermal electron scattering model may capture the τ_e weighted mean temperature of the electron scattering medium, which is rather close to the $T_e \simeq 1.1 \times 10^4$ K derived above.

4.3. *Is it really electron scattering?*

Although our best fit model parameters, T_e and τ_e, are tightly constrained by the observed Hα profile, it is not clear that this model is the only possible interpretation. One may assume that no electron scattering is present, and that the Hα gas emissivity as a function of velocity in the BLR just happens to produce an exponential profile. How can the electron scattering model be tested? A clear prediction of our model is that τ_e should be tightly correlated with the ionizing flux. As the ionizing flux

increases the column of ionized gas must increase, and the relative fraction of line flux in the scattering wings should increase. If the BLR gas has a large column, so it is ionization bounded rather than matter bounded, then the relation between τ_e and the ionizing flux should be linear. In contrast, the slope of the exponential wings σ should remain nearly constant. This occurs since T_e is only weakly dependent on U (for $U < 1$), and thus should vary only slightly. In addition, although τ_e is expected to vary linearly with U, σ is only weakly dependent on τ_e, and would thus not be significantly affected. The ionization structure responds on a timescale of $\sim 4 \times 10^{12}/n_e$ seconds, or ~ 400 seconds for the BLR, which is much smaller than the BLR light crossing time of ~ 1 hour (Peterson et al. 2005). Thus, one expects the measured τ_e and T_e to respond to changes in the ionizing continuum on timescales as short as ~ 1 hour. However, since the dynamical time in the BLR of NGC 4395 is ~ 1 week, structural changes may occur on this time scale, or longer, which could eliminate the correlation of τ_e and T_e with the ionizing flux (e.g. due to changes in the BLR density and column density).

Indirect evidence for electron scattering in NGC 4395 is provided by the spectropolarimetry of Barth et al. (1999), who find a wavelength independent polarization of $0.67 \pm 0.03\%$. The similar low polarization of the continuum and the broad lines suggests the scattering most likely occurs by a low τ_e scattering medium outside the BLR, rather than within the BLR gas, as suggested here [1]. Barth et al. suggested that "A clear sign of electron scattering would be a broadened Hα profile in Stokes flux,". The exponential Hα wings revealed in this study are probably not related to the Barth et al. prediction, unless scattering off the BLR clouds can produce the observed continuum and line polarization (Korista & Ferland 1998). Spectropolarimetry at a higher S/N and higher spectral resolution is required to better constrain the location and identity of the polarizing medium in NGC 4395.

Indirect support for the electron-scattering-within-the-BLR interpretation is provided by the fact that best fit values of the two free model parameters, T_e and τ_e, can apparently be obtained using a single parameter, $U \sim 0.3$. This value of U is consistent with the range of U values typically deduced in AGN, though it is significantly higher than deduced by Kraemer et al. (1999) for this object. Can the required U and $\Sigma_{\rm H}$ be accommodated within the small BLR of NGC 4395? To estimate the physical size of such a BLR component we use the mean "visit 3" flux density of $f_\lambda = 3 \times 10^{-15}$ erg^{-1} s^{-1} cm^{-2} Å^{-1} at 1350Å, taken from Table 3 in Peterson et al. (2005, note an Erratum with corrected flux), which matches well an extrapolation of our ESI spectrum to the UV. At a distance of 4.3 Mpc (Thim et al. 2004), the corresponding monochromatic luminosity is $\lambda L_\lambda = 1.05 \times 10^{40}$ erg^{-1} s^{-1}, corrected for Galactic extinction of 0.175 mag at 1350Å (Schlegel et al. 1998 and Table 1 in Mathis 1990). Assuming the ionizing luminosity is $\simeq 3\lambda L_\lambda$ at 1350Å, and a mean ionizing photon energy of $\simeq 2$ Rydberg, the implied ionizing

photon flux from the source is $\dot{N} \simeq 7 \times 10^{50}$ s^{-1}. Using $U \equiv \dot{N}/(4\pi r^2 c n_e)$ we get $U \simeq 20 r_{14}^{-2} n_{10}^{-1}$, where the distance of the emitting gas is $r = 10^{14} r_{14}$ cm, and its density is $n_e = 10^{10} n_{10}$ cm^{-3}. The measured value of $U = 0.3$ implies a distance $r_{14} = 8 n_{10}^{-0.5}$. The thickness of the gas slab is $d_{14} = \Sigma_{24}/n_{10}$ cm, and thus for $\Sigma_{24} = 1$ found here we get $d/r = 0.12 n_{10}^{-0.5}$. Therefore, $d/r \lesssim 0.1$ for $n_e \gtrsim 10^{10}$ cm^{-3}, and the implied column of Hα emitting gas can be accommodated within the compact BLR of NGC 4395, for reasonable values of n_e.

Why then are such exponential wings not commonly seen in other AGN? NGC 4395 is unique among type I AGN in having extremely narrow Balmer lines. The broad Hα FWHM here is just 520 km s^{-1}, while the typical Hα FWHM in AGN is ~ 3000 km s^{-1}, with a few times broader line base. Thus, the electron scattering effect of the BLR gas will have a negligible effect on the emission line width in most AGN. However, one can make a clear prediction that the exponential wings should be discernable in other objects with unusually narrow lines. A reliable detection of such wings requires a high S/N spectrum (e.g. 10-70 here at $1000 < |v| < 2500$ km s^{-1}). For example, the Hβ line wings of NGC 4395, and the Hα line wings in a Keck spectrum of POX 52 (Barth et al. 2004, kindly provided by A. Barth), are broadly consistent with an exponential form, but the available S/N in both cases is too low to constrain the profile shape as accurately as done here. We note in passing that as long as τ_e remains low ($\lesssim 0.5$), electron scattering would not have a significant effect on measurements of the line FWHM, and thus on estimates of the black hole mass (e.g. Kaspi et al. 2005).

5. CONCLUSIONS

High quality Keck observations of the Hα line in NGC 4395 reveal symmetric exponential wings of the form $f_v \propto e^{-v/\sigma}$, with $\sigma \simeq 500$ km s^{-1}. The wings are fit well by an isothermal and isotropic electron scattering model with $\tau_e = 0.34$, and $T_e = 1.14 \times 10^4$K, plausibly generated in photoionized gas with $U \simeq 0.3$. The lack of electron scattering wings for the [O III] $\lambda 5007$ line, and the value of U indicate that the scattering occurs within the BLR gas where Hα is formed.

The electron scattering interpretation can be tested by looking for a strong correlation between τ_e and the ionizing flux. High quality spectra of other AGN with very narrow Balmer lines will provide a further test of the electron scattering interpretation. If the electron scattering origin is verified, then the extended Hα wings can provide us with a new direct probe of T_e and τ_e within the BLR gas, and their time variability.

[1] Inspection of the 2-D spectral images of NGC 4395 obtained with the HST STIS suggests some spatially extended scattered nuclear light.

REFERENCES

Antonucci, R. 1993, ARA&A, 31, 473

Barth, A. J., Filippenko, A. V., & Moran, E. C. 1999, ApJ, 525, 673

Barth, A. J., Ho, L. C., Rutledge, R. E., & Sargent, W. L. W. 2004, ApJ, 607, 90

Bottorff, M., Korista, K. T., Shlosman, I., & Blandford, R. D. 1997, ApJ, 479, 200

Chandrasekhar, S. 1960, Radiative Transfer, New York: Dover, 1960,

Davidson, K., & Netzer, H. 1979, Reviews of Modern Physics, 51, 715

Emmering, R. T., Blandford, R. D., & Shlosman, I. 1992, ApJ, 385, 460

Ferrarese, L., Pogge, R. W., Peterson, B. M., Merritt, D., Wandel, A., & Joseph, C. L. 2001, ApJ, 555, L79

Ferland, G. J., Korista, K. T., Verner, D. A., Ferguson, J. W., Kingdon, J. B., & Verner, E. M. 1998, PASP, 110, 761

Kallman, T. R., & Krolik, J. H. 1986, ApJ, 308, 805

Kaspi, S., Maoz, D., Netzer, H., Peterson, B. M., Vestergaard, M., & Jannuzi, B. T. 2005, ApJ, 629, 61

Korista, K., & Ferland, G. 1998, ApJ, 495, 672

Kraemer, S. B., Ho, L. C., Crenshaw, D. M., Shields, J. C., & Filippenko, A. V. 1999, ApJ, 520, 564

Laor, A. 1998, ApJ, 505, L83

Laor, A., Barth, A. J., Ho, L. C., & Filippenko, A. V. 2006, ApJ, 636, 83

Lee, H.-W. 1999, ApJ, 511, L13

Mathis, J. S. 1970, ApJ, 162, 761

Mathis, J. S. 1990, ARA&A, 28, 37

Mathews, W. G., & Ferland, G. J. 1987, ApJ, 323, 456

Mihalas, D. 1978, Stellar Atmospheres, San Francisco, W. H. Freeman and Co., 1978. 650 p.,

Miller, J. S., Goodrich, R. W., & Mathews, W. G. 1991, ApJ, 378, 47

Moran, E. C., Filippenko, A. V., Ho, L. C., Shields, J. C., Belloni, T., Comastri, A., Snowden, S. L., & Sramek, R. A. 1999, PASP, 111, 801

Peterson, B. M., & Wandel, A. 2000, ApJ, 540, L13

Peterson, B. M., et al. 2005, ApJ, 632, 799

Rees, M. J., Netzer, H., & Ferland, G. J. 1989, ApJ, 347, 640

Rybicki, G. B., & Lightman, A. P. 1979, Radiative Processes in Astrophysics, New York, Wiley-Interscience, 1979. 393 p. (RL79)

Schlegel, D. J., Finkbeiner, D. P., & Davis, M. 1998, ApJ, 500, 525

Sheinis, A. I., Bolte, M., Epps, H. W., Kibrick, R. I., Miller, J. S., Radovan, M. V., Bigelow, B. C., & Sutin, B. M. 2002, PASP, 114, 851

Shields, G. A., & McKee, C. F. 1981, ApJ, 246, L57

Thim, F., Hoessel, J. G., Saha, A., Claver, J., Dolphin, A., & Tammann, G. A. 2004, AJ, 127, 2322

Weymann, R. J. 1970, ApJ, 160, 31